ADVANCED FUNCTIONAL MATERIALS
www.afm-journal.de

Advancing Hydrovoltaic Energy Harvesting from Wood through Cell Wall Nanoengineering

*Jonas Garemark, Farsa Ram, Lianlian Liu, Ioanna Sapouna, Maria F. Cortes Ruiz, Per Tomas Larsson, and Yuanyuan Li**

Converting omnipresent environmental energy through the assistance of spontaneous water evaporation is an emerging technology for sustainable energy systems. Developing bio-based hydrovoltaic materials further pushes the sustainability, where wood is a prospect due to its native hydrophilic and anisotropic structure. However, current wood-based water evaporation-assisted power generators are facing the challenge of low power density. Here, an efficient hydrovoltaic wood power generator is reported based on wood cell wall nanoengineering. A highly porous wood with cellulosic network filling the lumen is fabricated through a green, one-step treatment using sodium hydroxide to maximize the wood surface area, introduce chemical functionality, and enhance the cell wall permeability of water. An open-circuit potential of ≈140 mV in deionized water is realized, over ten times higher than native wood. Further tuning the pH difference between wood and water, due to an ion concentration gradient, a potential up to 1 V and a remarkable power output of 1.35 µW cm^{-2} is achieved. The findings in this study provide a new strategy for efficient wood power generators.

1. Introduction

Efficient energy harvesting from clean energy sources is attractive for sustainable energy systems. Electric power generation from water is getting increasing attention ascribing to the enormous amount of embedded clean energy, ≈35% of which is solar energy received by Earth.[1] Although with current success such as hydropower technology, the amount of energy harnessed is still far from satisfactory. Recent advances in nanotechnology stimulate the development of new water energy harvesting technologies that are less bound to geographical locations and infrastructure.[2] These technologies rely on the hydrovoltaic effect, which is the generation of an electrical potential at the interphase of water and polarizable materials,[1,3] and has been demonstrated through waves,[4] water evaporation,[5] moisture-sorption,[6] and droplets.[7] Amongst these technologies, water evaporation-induced electricity is especially attractive, as the water evaporation process is spontaneous and engages two-third of water energy, it can offer continuous electricity generation without a specific environmental stimulus.

By passing water through porous media assisted by water evaporation, a streaming current and voltage can be achieved due to the presence of an electric double layer (EDL) at the solid–liquid interface.[8] This is called the electrokinetic effect.[8b,9] On the basis of the mechanisms, various materials have been investigated to harvest energy. Early on, electricity generation by natural evaporation was reported on porous carbon substrates.[5] Since then, many types of devices have been formed, including porous carbon-materials,[3a,5,10] metal oxides,[11] bio materials,[12] etc. Impressive open circuit potentials of >1 V were reported.[5,10a,b,11a] However, the power density is inferior ascribing to the high resistance to water flow and weak interaction between water and materials. Advanced materials design could provide solutions. The design principles include maximizing the contact area with water, improving the charge separation ability, and boosting the water flow. Therefore, materials with high nano-porosity, good water wettability, charged surface, and desirable transportation properties are demanded. Renewable material resources are sought for, considering the sustainability aspects.

J. Garemark, F. Ram, L. Liu, I. Sapouna, M. F. Cortes Ruiz, P. T. Larsson, Y. Li
Wallenberg Wood Science Center
Department of Fiber and Polymer Technology
KTH Royal Institute of Technology
Stockholm SE-10044, Sweden
E-mail: yua@kth.se

I. Sapouna
Division of Glycoscience
Department of Chemistry
KTH Royal Institute of Technology
AlbaNova University Centre
Stockholm 106 91, Sweden

P. T. Larsson
RISE AB
Drottning Kristinas Väg 61, PO. Box 5604, Stockholm SE-114 86, Sweden

The ORCID identification number(s) for the author(s) of this article can be found under https://doi.org/10.1002/adfm.202208933.

DOI: 10.1002/adfm.202208933

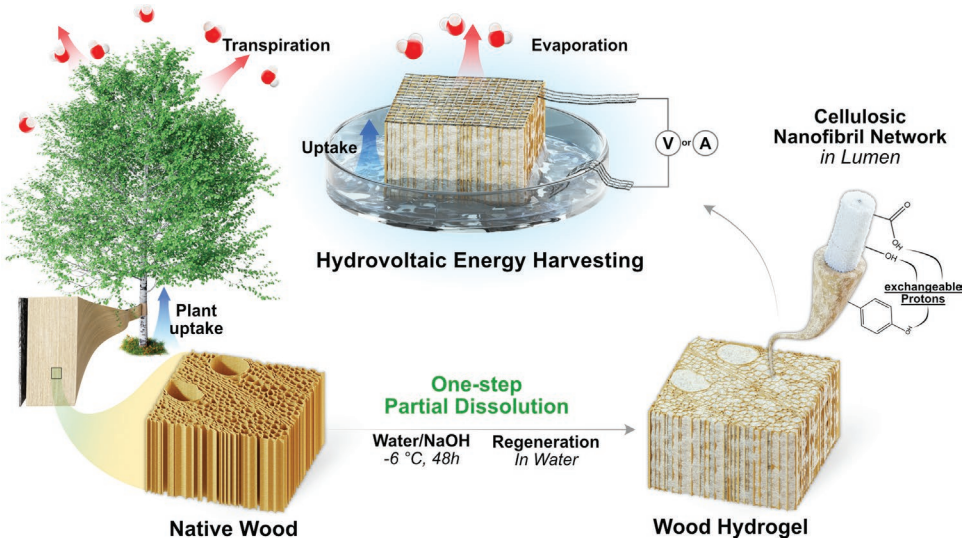

Figure 1. Schematic of the formation of wood power generators. The left-hand side depicts the natural water uptake and transpiration of wood and its hierarchical structure. From the native wood, the one-step treatment is shown, leading to wood with precipitated nanofibrillated networks within the lumen and its abundance of functional groups. The final hydrovoltaic energy harvester is shown under operation. Blue arrow refers to water uptake and red arrow represents water evaporation. ● represents water molecules.

Nature designs well-structured water conductors in plants. Owing to the porous and anisotropic structure of aligned biopolymers rich in polar functionalities (hydroxyls, carboxyls, and phenols), wood can be used as an evaporation-assisted electric power generator. In earlier works, wood functionalization,[12b] and metal salt doping of wood carbons[12c] have been investigated. However, the advantage of the empty wood channels (lumen) was not fully explored since the empty wood channels can reach up to 200 µm in diameter, whereas the EDL thickness can be <1 nm at high salt concentrations.[13] Furthermore, the accessibility of wood biopolymers is limited by permeability of the compact cell walls.

Previously, we developed a non-additive strategy to improve wood surface area and permeability via cell wall nanoengineering, partial dissolution of the wood cell wall, and transfer of biopolymers to the lumen in the form of nanostructured networks.[14] In pursuit of eco-friendly materials, a shift to greener chemicals is necessary. One of the most benign is the water/NaOH system, which has cellulose dissolution capabilities at sub-zero temperatures.[15] NaOH is also known for its ability to scission lignin, leading to more available phenolic content, which is beneficial for hydrovoltaic energy harvesting.[16]

Therefore, in this work, we prepared highly porous wood (nanoengineered wood) via a one-step treatment of wood using NaOH for high-performance hydrovoltaic power generators. The formed mesoporous structure with nanoporous cellulosic networks in the lumen leads to high specific surface areas (SSA) > 180 m^2 g^{-1} and beneficial chemical functionalities could respond to pH-induced charge dissociation. The devices based on the nanoengineered wood could reach an impressive potential of 140 mV in deionized (DI) water. Under alkali conditions (pH 13.4), a steady open circuit potential (V_{oc}) of ≈550 mV and a short circuit current (I_{sc}) of ≈7 µA were obtained. With further increase in pH difference of the water reservoir (pH 13.4) and wood (pH 1), a V_{oc} of ≈1 V was achieved leading to a remarkable power density of 1.35 µW cm^{-2} (**Figure** 1).

2. Results and Discussion

2.1. Morphology and Composition

Highly porous nanoengineered wood for hydroelectricity harvesting was prepared through a one-step chemical treatment by immersing native wood (NW) into a water/NaOH mixture for 48 h at −6 °C. Lignin-free porous wood was also prepared as a reference to verify the role of lignin by delignification, called delignified wood (DW). These were further treated by the NaOH treatment (DW-NaOH). During partial dissolution, the wood cell wall substances partly solubilize and diffuse to the lumen. Upon addition of water, the solubilized substances precipitate, forming a nanofibrillated cellulosic structure within the before empty lumen and a porous remaining cell wall, see **Figure 2**a–d. The fibrillation density was remarkably high, seen in high magnification image of Figure S1 (Supporting Information). SEM images of DW and native birch wood (NBi) can be seen in Figure S2 (Supporting Information). NBi does not dissolve as readily as native balsa wood (NBa). Therefore, NaOH-treated NBi (NBi-NaOH) exhibits less network density in the lumen compared to NaOH-treated NBa (NBa-NaOH) (Figure 2b,c). During the process, ≈20 wt.% materials loss was observed for NBa and NBi, see Table S1 (Supporting Information). This is a great improvement considering materials efficiency compared to ≈50% weight loss in the previously reported works.[14] Relative hemicellulose content decreased 4 wt.% for NBa-NaOH compared with NBa, whereas DW-NaOH only had ≈1 wt.% remaining (Figure 2f). On the other hand, NBi-NaOH exhibits no reduction in hemicellulose, this could be due to limited penetration of the thick cell walls of NBi. Even though weight loss was observed, NBa-NaOH shows increased density (156 kg m^{-3} for NBa to 162 kg m^{-3} for NBa-NaOH) as regeneration led to shrinkage. Similar phenomenon was observed for treated delignified balsa wood (DW-NaOH), seen in Figure 2e. Different trend is noticed for NBi-NaOH due to less structure shrinkage.

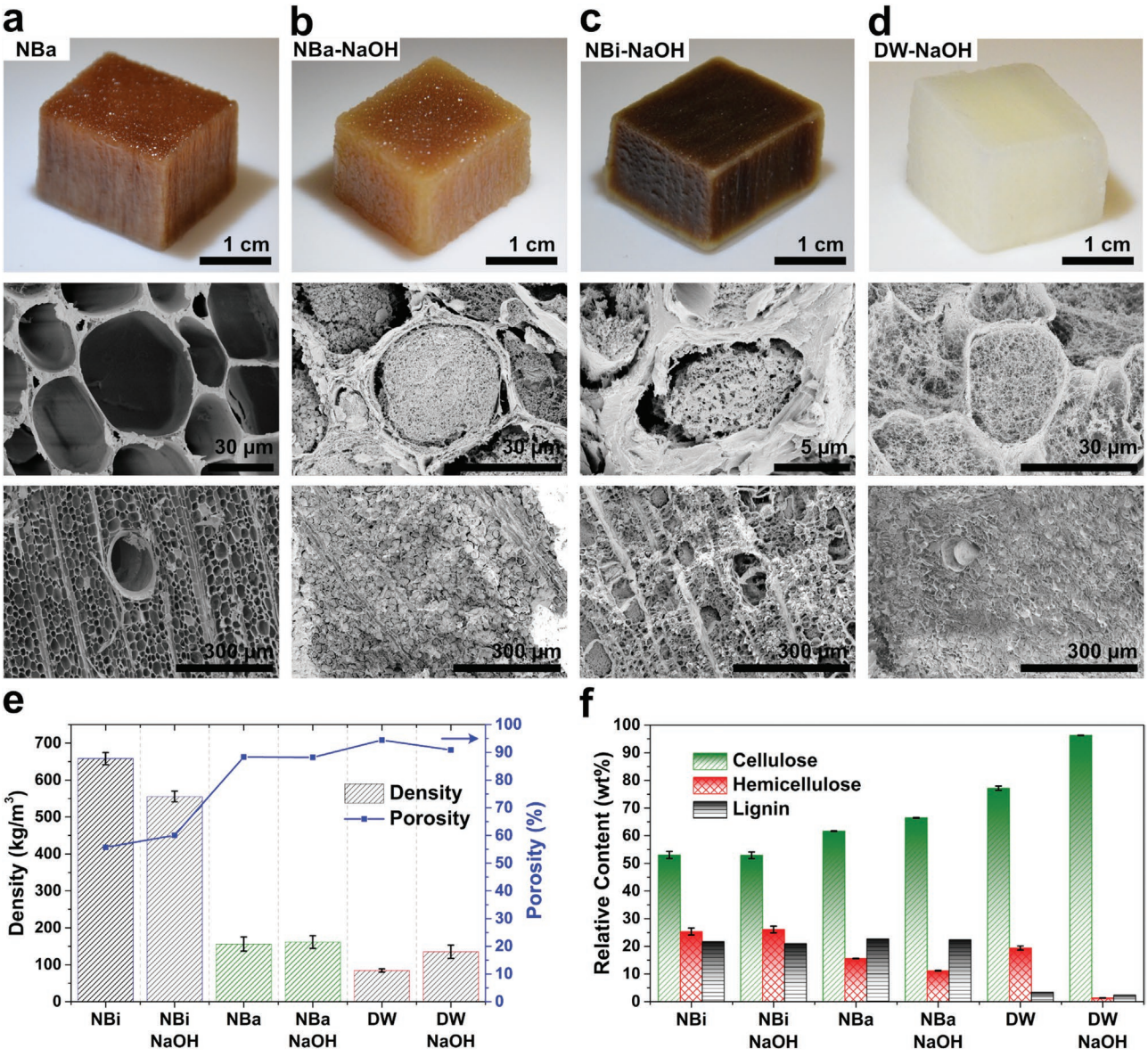

Figure 2. a–d) morphology of wood samples (NBa, NBa-NaOH, NBi-NaOH, and DW-NaOH), e) density and porosity of all wood samples, and f) carbohydrate and lignin content of all wood samples.

Increasing the contact area between wood and water plays an important role in hydrovoltaic energy harvesting. Therefore, SSA and pore-size distribution (PSD) was thoroughly investigated by using small angle x-ray scattering (SAXS) and Brunauer-Emmett-Teller (BET) nitrogen physisorption. SAXS has the advantage to "see" the never-dried structure, which is difficult to study under microscopes without disturbing the structure. 2D scattering patterns in **Figure 3**a show high anisotropic scattering of the natural woods (NBa and NBi) and DW. The subsequent hydrogel formation leads to less anisotropy indicated by the scattering signals (Figure 3a), interpreted as being due to the random nanofibril network formation in the lumen. Figure 3b shows intensity versus scattering vector (q) relationship where NBa and NBi have signals at ≈1.6 nm^{-1} corresponding to the inter-fibril correlation length of ≈4 nm (Figure 3e). This could be assigned to the correlation of oriented cellulose microfibrils in the cell walls.[17] The inter-fibril correlation length slightly increased for DW due to the swelling of the cell wall structure after lignin removal. After NaOH treatment, the relationship changed, where the signal at ≈1.6 nm^{-1} decreased (Figure 3a), indicating a significant structure change. By plotting an $I(q)q^2$ versus q profile, a clear signal suggesting size between 10–20 nm was observed, which mainly is understood as the porosity of the nanofibrillated networks in lumina, but also from the obtained nanoporosity of the cell walls after treatment, see inset SEM images of Figure 3f,g. The apparent decrease of the inter-fibril correlation signal in the NBa-NaOH, NBi-NaOH, and DW-NaOH samples, could be the result of a larger separation of cell wall microfibrils due to swelling or as a result of a relatively lower volume fraction of highly correlated

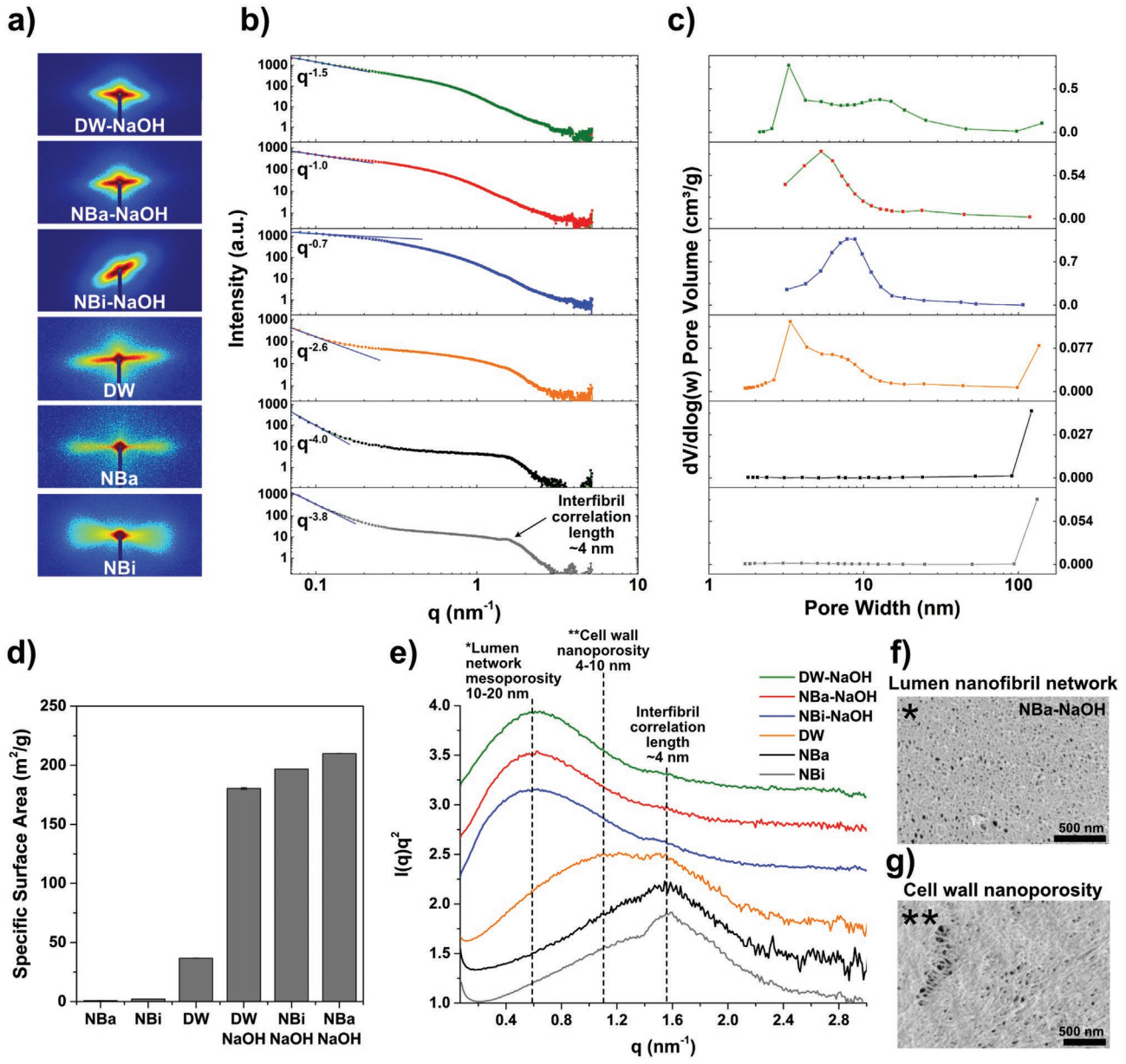

Figure 3. a) 2D Small angle X-ray diffraction patterns and b) corresponding 1D scattering line profiles of wood samples (NBa, NBi, DW, NBi-NaOH, NBa-NaOH, and DW-NaOH) in water, c) physisorption pore-size distribution and d) specific surface area of NBa, NBi, DW, NBi-NaOH, NBa-NaOH, and DW-NaOH, e) Kratky plot for NBa, NBi, DW, NBi-NaOH, NBa-NaOH, and DW-NaOH. Inset SEM images are nanofibril network in the lumen of NBa-NaOH and cell wall structure of NBa-NaOH.

fibrils due to the formation of the random fibrillar network in the lumen. A high mesoporosity is observed for NBi-NaOH and NBa-NaOH, also seen in pore-size distribution of nitrogen physisorption of Figure 3c. Fitting at low q-values (power law), a slope of $\approx q^{-4}$ was seen for NBa and NBi, which could be assigned to the surfaces of large pores and fiber lumina.[17b,18] The NaOH-treated wood showed significantly different characteristics as slopes decreased to $q^{-0.7}$ and q^{-1} for NBi-NaOH and NBa-NaOH, respectively, likely describing smaller aggregation sizes and lower relative amount of aggregated structures. A q^{-1} has been described as rod-like structure that fits the description of the observed nanofibrillated networks of the fiber lumina.[19] The $q^{-2.6}$ from DW likely describes a mixed structure as delamination of the cell wall and nanoporosity transpires, small pores in the cell wall and large empty lumina. The mixed structure likely translated to DW-NaOH as a $q^{-1.5}$ was observed, potentially representing a rod (nanofibrils) and plate-like (delaminated cell wall) structure.

With the significantly increased nanoporosity and nanofibril networks, SSA of all wood aerogels is vastly enhanced. The SSA for NBa, NBi, and DW are 1, 2, and 37 $m^2\ g^{-1}$, respectively, while the values are 210, 196, and 180 $m^2\ g^{-1}$ for NBa-NaOH, NBi-NaOH, and DW-NaOH, respectively. Physisorption isotherms can be seen in Figure S3 (Supporting Information). The

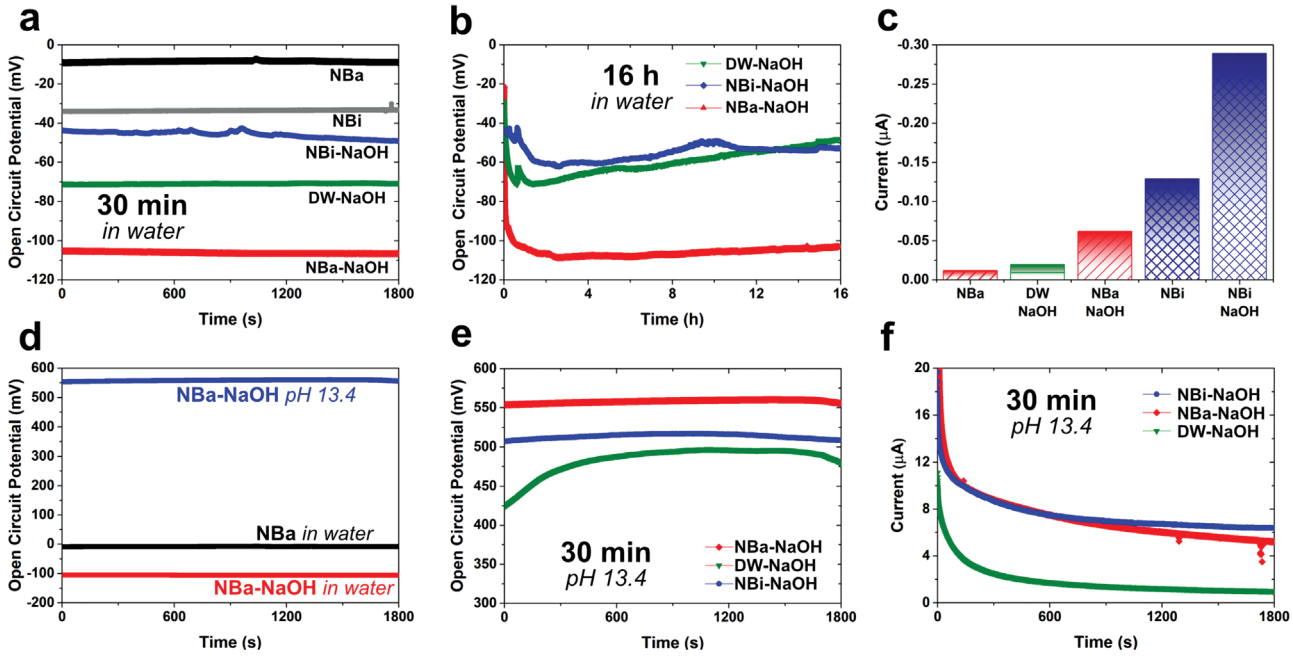

Figure 4. a) V_{oc} comparison of NBi, NBa, DW-NaOH, NBi-NaOH, and NBa-NaOH samples with area of 1.5 cm^2 in DI water after reaching stable values, measured for 30 min. b) V_{oc} of treated samples for 16 h in DI water from the beginning. c) the constant I_{sc} for all the samples in DI water. d) V_{oc} of NBa and NBa-NaOH in DI water and in pH 13.4 NaOH reservoir. e) V_{oc} of the NaOH treated samples in pH 13.4 NaOH reservoir for 30 min. f) I_{sc} of NaOH treated samples in pH 13.4 NaOH reservoir for 30 min from the beginning.

substantial increase in SSA maximizes the effective contact area with water, which is highly beneficial for power generation.

2.2. Electricity Generation and Optimization

Hydrovoltaic electricity harvesting derived from spontaneous water evaporation using the wood samples (1 × 1.5 cm^2) was demonstrated. The V_{oc} and I_{sc} were evaluated, shown in **Figure 4**a–f. When stable V_{oc} was reached, 30 min measurements followed, in which –10 and –33 mV were recorded for NBa and NBi, when operating in DI water, respectively (Figure 4a). The higher potential of NBi could be attributed to the smaller micro-channels compared to NBa, inducing a larger pressure difference.[12b] Equations S1 and S2 in the Supporting Information show the influence of lumen diameter on streaming potential. Significant performance improvements were observed for NaOH-treated samples. V_{oc} of NBi-NaOH increased to ≈–50 mV, whereas NBa-NaOH showed a remarkable 10-fold increase in potential to ≈–105 mV. The substantial increase could be ascribed to the high SSA (Figure 3d), nanoporosity (Figure 2e), and surface charge of NaOH-treated samples. **Table 1** shows the surface charge of the samples. NaOH treatment on native wood generally resulted in higher surface charge density reflected by the increase from 38 μmol g^{-1} (NBi) to 123 μmol g^{-1} for NBi-NaOH and from 139 μmol g^{-1} (NBa) to 267 μmol g^{-1} for NBa-NaOH. Zeta(ζ)-potential follows the same trend of surface charge (Table 1). The increased surface charge could be assigned to an increase of phenolic-OH (from 630 to 710 μmol g^{-1} for both NBi-NaOH and NBa-NaOH) mainly due to breaking of β-O-4′ linkages (β-O-4′ content reduced from 65% to 56% of NBa-NaOH) in lignin during NaOH treatment. Figures S4 and S5 and Table S2 (Supporting Information) show detailed lignin structure analysis. The assumption is further supported by decreased surface charge from 284 μmol g^{-1} for DW to 224 μmol g^{-1} for DW-NaOH, where lignin is nearly absent (≈1 wt.%). Interestingly, DW-NaOH shows a better performance than NBi-NaOH but worse than NBa-NaOH, indicating the critical role of both porosity and surface chemistry. Stable potential was achieved for the lignin-rich NBi-NaOH and NBa-NaOH over 16 h running (Figure 4b), whereas DW-NaOH slightly decreased over time. For I_{sc}, a correlation to density of the materials was seen, being significantly higher for NBi (≈–0.12 μA of NBi and ≈–0.01 μA for NBa) (Figure 4c). After NaOH treatment, NBi-NaOH exhibits the highest I_{sc} with a value of ≈–0.28 μA. Drastically enhanced performance

Table 1. As-prepared wood surface charge and ζ-potential of samples in water at pH 7.

	DW	DW-NaOH	NBi	NBi-NaOH	NBa	NBa-NaOH
Surface charge [μmol g^{-1}]	284 ± 5	224 ± 20	38 ± 3	123 ± 22	139 ± 6	267 ± 56
ζ-potential [mV]	–31 ± 2	–27 ± 1	–33 ± 1	–48 ± 2	–32 ± 1	–42 ± 2

was achieved when wood samples were introduced to a pH 13.4 NaOH electrolyte reservoir, see Figure 4d. 30 min runs showed a V_{oc} of ≈550 mV for NBa-NaOH. The V_{oc} is ≈500 and ≈480 mV for NBi-NaOH and DW-NaOH, respectively, as shown in Figure 4e. Hence, the V_{oc} increased 55-fold from NBa in water to NBa-NaOH in the NaOH reservoir. The substantially higher performance achieved in the electrolyte is due to ion diffusion caused by an ion concentration gradient over wood. In electrolyte, water evaporation contributes less to the overall performance, although is important as it compensates for the loss in water due to evaporation. Increased I_{sc} of ≈7 μA was obtained for NBi-NaOH and NBa-NaOH, seen Figure 4f. The improved current for NBa-NaOH is partly attributed to the faster chemical diffusion, which could arise from the higher SSA and lower density. The higher surface charge of NBa-NaOH is believed to be beneficial for higher currents as more dissociation of functional groups can transpire. DW-NaOH shows obvious performance deterioration over time in both water and alkali as seen in Figure 4b,e. Possible reason is that wood swells significantly in water and alkali, leading to structure collapse. Preservation of lignin in the wood is key to prevent cumbersome swelling and performance deterioration. This is supported by the better stability of NBa-NaOH and NBi-NaOH. Given the excellent performance and stability, NBa-NaOH was used to further understand the mechanisms.

It was noticed that the state of the wood surface functional groups influenced the power generation. In wood, carboxylic acids of hemicellulose and phenolic groups in lignin are the main contributors to surface charge. As-prepared NBa-NaOH (NBa-NaOH (as-prepared)) is slightly basic even when kept in water for a long duration, due to the dissociated carboxylic acid groups. When run in a NaOH reservoir of pH 13.4 the V_{oc} obtained was ≈200 mV, seen in **Figure 5**a. When the same sample was protonated by pre-treatment in an HCl solution and washed (pH of the protonated wood is 5) prior to running in pH 13.4 a V_{oc} of ≈550 mV was recorded, which is a near 3-fold improvement compared to as-prepared NBa-NaOH working at pH 13.4. Simultaneously, the current reached a high value of ≈7 μA, compared to as-prepared of ≈2 μA (Figure 5b). The highest V_{oc} could be sustained for a few hours, see Figure S6 (Supporting Information), followed by slow decrease to ≈50 mV after ≈6 h. However, NBi-NaOH showed a more stable decrease with time, likely due to the higher density (Figure S10, Supporting Information). This is significant since the mix of high V_{oc} and I_{sc} can be sustained for a considerable amount of time. The eventual performance drop could be due to depletion of protons throughout the wood, a similar ionic strength between the wood and the reservoir, and suppression of the EDL due to high counterion concentration. The details are described in the mechanisms discussion. It should be noted that, the deprotonated samples after running could be protonated in weak acid again. Cycles > 10 times (equivalent to ≈40 h) showed neither deterioration of the structure nor loss in performance, see Figure 5c. FT-IR provides further insight on mechanisms. As-prepared NBa-NaOH showed the carboxylate form of functional groups. Upon acid treatment, the groups were protonated that was seen from the signal ≈1740 cm^{-1} in Figure 5d. After 16 h run in pH 13.4 alkali reservoir the carboxylate signal returns. Full FT-IR spectra (Figure S7, Supporting Information) show no degradation of the materials. SEM images of a NBa-NaOH sample after 16 h run in alkali reservoir (pH 13.4) show no significant structure change, and can be seen in Figure S8 (Supporting Information). This observation is in agreement with literature as low alkali concentration in room temperature is benign to the biopolymers.[20] However, at elevated temperature, even low concentration alkali could degrade both lignin and carbohydrates.[21]

A pH dependent device performance was observed. Figure 5e shows V_{oc} from NBa-NaOH running in water with different pH. Comparable V_{oc} was obtained when pH was 1 (≈–125 mV) and 7 (≈–110 mV). Further increasing pH, the V_{oc} first decrease and then increase where the potential direction inverted at pH 12. Maximum V_{oc} with a value of ≈550 mV was obtained at pH 13.4. Curves for V_{oc} at different pH are seen in Figure S9 (Supporting Information).

The surface charge plays an important role in improving potential difference and thus current over wood and a critical role of lignin was noticed by analyzing lignin contribution to ζ-potential through ζ-potential titrations (Figure 5f). Both DW-NaOH and NBa-NaOH show an initial slope between pH 2–4, representing deprotonation of carboxylic acid (pKa ≈ 4.6). Thereafter, a linear curve of low slope was obtained for DW-NaOH. NBa-NaOH shows different behavior, where a rapid ζ-potential increase after pH 10 was seen. This response is ascribed to phenol deprotonation (pKa ≈ 10) of lignin constituents.

The difference in pH between the wood sample and reservoir was understood as a key aspect of the obtained V_{oc}. This was justified by submerging wood in an acid (HCl) of pH 1, followed by placing it in an alkali (pH 13.4) reservoir, as seen in Figure 5g. Full 16 h curve is found in Figure S10 (Supporting Information). This gave a remarkable V_{oc} of 1 V compared to 500–550 mV that was achieved from protonated wood (pH ≈ 5). This aspect has thus far been overlooked for water evaporation-driven energy harvesting from wood in literature,[12b,c] which becomes critical as wood can be either acidic or basic depending on their treatment prior to energy harvesting. Moreover, the current increase substantially at the same time, as seen in Figure S11 (Supporting Information). Description of the different NBa-NaOH sample of varying pH is summarized in Table S3 (Supporting Information).

2.3. Mechanisms Understanding

When water passes through a porous media driven by water evaporation, a continuous streaming current and potential can be achieved due to the presence of an EDL at the solid–liquid interface,[8a] which can be described by the phenomenon of electrokinetics.[8b,9] The hydrovoltaic electricity generation in wood is influenced by several factors including the materials SSA, porosity, surface charge/ζ-potential, water transportation in the porous media, and the water solution. Porous cell walls and mesoporous fibrillated networks in NaOH-treated wood show high SSA and porosity, inducing strong capillary forces. The net negative surface charge of the treated wood is surrounded by positive counterions that forms into an EDL. This layer consists of two regions, the inner of immobile counterions

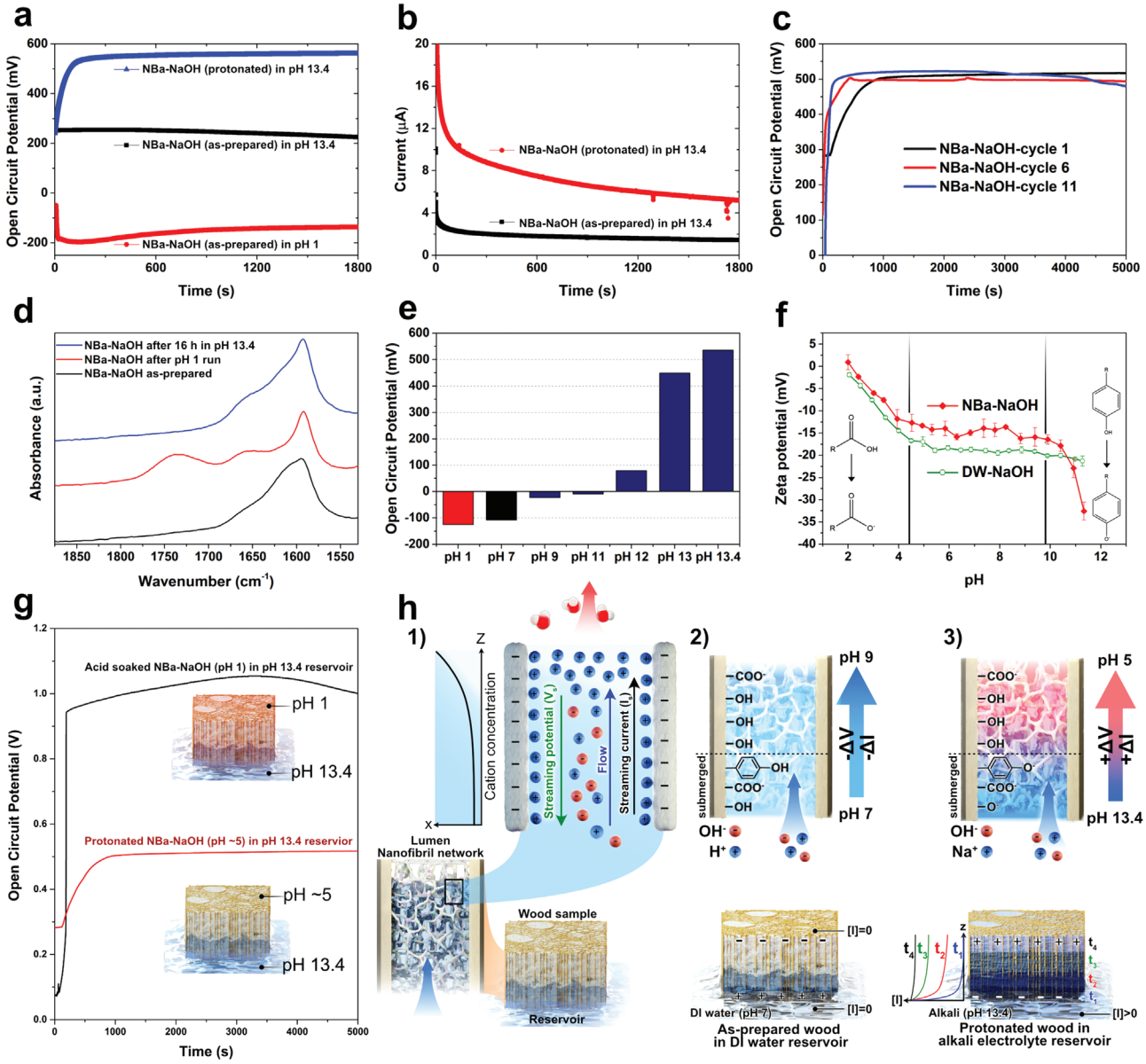

Figure 5. a) the effect on V_{oc} upon protonation prior to run in pH 13.4 alkali reservoir and b) subsequent effect on I_{sc}. c) cyclability of NBa-NaOH samples in pH 13.4 alkali solution. d) FT-IR of protonation/deprotonation mechanism, e) V_{oc} at different pH, where red represents pH adjustment with HCl and navy blue with NaOH. f) shows ζ-potential under titration for NBa-NaOH & DW-NaOH. g) V_{oc} comparison of large pH difference between wood (pH 1) and reservoir (pH 13.4) and smaller (pH 5 to pH 13.4). h) 1) Illustration of the wood sample in a reservoir with a zoom-in of the nanofibrillated networks and evaporation-assisted flow that, due to the build-up of counterions, lead to overlapping EDLs where counter-ion flow gives rise to a streaming current (I_s) and potential (V_s). Left-hand side curve shows the cation concentration over z and x-axis. 2) shows the as-prepared wood in a water-reservoir. 3) shows the proposed mechanisms when protonated wood is placed in an alkali reservoir. In 2) and 3) the [I] represents the ion concentration and t1, t2, t3, and t4 represent points in time. The inset curves describe the change in ion concentration with respect to time (t) and the height of the wood samples (Z-axis). Molecular groups are exaggerated for visual aid.

(stern layer) and the outer of mobile counterions (diffuse layer).[8b] The distribution of charges of the diffuse layer with respect to the bulk brings about an electrical potential and the potential at the shear plane is called the ζ-potential.[22] Through the sample, a constant capillary flow is achieved due to the continuous water evaporation at the liquid/air interface, to compensate for the loss of water.[8b,11b] This hydrodynamic flow gives rise to a drag of ions along the diffuse layer of fibrillar networks and cell walls and a streaming current is formed in the direction of the hydrodynamic flow.[8a,23] A charge polarization over the porous wood occurs that results in movement of charge that opposes the flow direction, called conduction current. Upon steady-state, the streaming and conduction current are equal and the maximum streaming potential is established over the wood. These mechanisms for electricity generation are seen in Figure 5h.[8a,9,12b,23]

In the case of as-prepared samples in a DI water reservoir, the wood will have a local basic pH due to the hydrogel treatment in strong alkali, even when thoroughly washed in water of pH 7. Consequently, the EDL is significant given the ζ-potential around pH 9–10 (Figure 5f). The water evaporation-assisted flow leads to upward transportation of water molecules and auto-dissociation of water ensures electroneutrality over the wood. Hence, in neutral DI water the electrokinetic effect assisted by natural water evaporation is the main contribution to energy generation. Figure 5h1 shows the built-up streaming potential and current and Figure 5h2 shows the proposed mechanisms for this case.

By utilizing a reservoir of NaOH (pH 9–13.4), the performance can be enhanced. Protonated samples placed in an alkali reservoir solution will start dissociating functional groups from the bottom and moving upward, as seen in Figure 5h3. As provided in Table 1, Table S2 (Supporting Information); Figure 5f, the abundant surface functional groups are a source of exchangeable protons (carboxylic acids, hydroxyls & phenols). The initial transportation of NaOH electrolyte is believed to create an ionization gradient as anions (carboxylate & phenoxides) remain immobile on the solid material.[12a,24] This upward ion diffusion and dissociation of functionality allow for a large potential difference (ion concentration difference) until the diffusion front reaches the top of the wood sample, as seen in Figure S12 (Supporting Information). When the top and bottom of wood have the same dissociated functional groups (same ionic strength), the potential and current start to decrease. Moreover, Na^+ screens the EDL that reduces its EDL overlap and decreases the performance. For this case, wood is seen as a dischargeable battery that can be recharged (protonated) repeatedly with the "discharge" lasting ≈3–8 h each time. The larger the pH difference over the wood, the larger the potential difference becomes. Hence, both the ionic strength of the reservoir and the wood surface charge are of great importance. For example, non-protonated (as-prepared) sample in an alkaline reservoir (pH 13.4) shows a potential of ≈200 mV (Figure 5a). A protonated wood (pH 5) in an alkaline reservoir (pH 13.4) reaches 500–550 mV (Figure 5a,g), and an acid-soaked wood (pH 1) placed in an alkaline reservoir (pH 13.4) reaches 1 V (Figure 5g). Evidently, electricity induced from evaporation has a low contribution when operating in electrolyte reservoirs. The ion diffusion was further elucidated as a temperature dependent V_{oc} was observed ascribing to the diffusion of electrolyte. Near 1 V was obtained when the reservoir was 60 °C compared to 0.55 V at room temperature. V_{oc} measurements under heating are seen in Figure S13 (Supporting Information).

The ionic strength and surface charge decide the sign of potential difference. If the pH of the wood is higher than the reservoir, a negative sign is seen and vice versa (Figure 5h2,h3). This justifies the negative sign when running as-prepared samples in water since the wood sample has a basic character due to dissociated carboxylic acids (≈pH 9), whereas the water reservoir is lower of pH 7 (Figure 5h3). This remains true for the case when NBa-NaOH is run in acid, where the top of the wood sample is significantly more basic than the submerged part in reservoir of pH 1.

2.4. Scaling of the Device and Demonstration

Scalability is critical to the practical applications of the devices. The nanofibrillated network formation within the lumen translated exceptionally to large area specimen. A device based on 4 × 4 cm^2 NBa-NaOH was assembled in water as shown in **Figure 6**a. A stable V_{oc} of ≈140 mV was recorded, which is even higher than that of 1.5 cm^2 samples. At the same time, an excellent I_{sc} of > 6 μA was obtained. From power density measurements, a maximum output power of ≈7 nW cm^{-2} was achieved for NBa-NaOH in water. When running in alkali, a V_{oc} of ≈550 mV and I_{sc} ≈7 μA was achieved leading to an output power of ≈0.62 μW cm^{-2}. This is one of the highest power outputs among a range of materials in literature through water evaporation[10a–c,e,11,25] (Figure 6c). Increasing the pH difference between wood (pH 1) and reservoir (pH 13.4) a V_{oc} of 1 V and I_{sc} ≈20 μA led to a remarkable maximum power output of 1.35 μW cm^{-2}. It should be noted that the maximum power was observed at an external load of ≈10^5 Ω in the circuit, which is lower than the native wood-based device. This could be assigned to the highly charged and aligned channels of open-ended porous networks with good capillary flow, which led to lower internal resistance. The I_{sc} and V_{oc} for hydrovoltaic devices reported in literature are summarized in Table S4 (Supporting Information).

The wood power generator could be used to power practical devices. Figure 6d shows an LED powered sustainably by six devices of 1.5 cm^2 based on NBa-NaOH connected in series. This setup was also able to power a timer with LCD screen, see Figure 6e. Continuously running the timer was achievable (Video S1, Supporting Information). The devices could also be used to charge a commercial capacitor for energy storage. Figure 6f shows the successful charging of a commercial capacitor with a capacity of 1000 μF to 2.2 V within 200–300 s (Figure 6f) using the wood power generator based on six pieces of NBa-NaOH with 1.5 cm^2 area (Video S2, Supporting Information). Based on biomass and green chemistry, wood power generator provides potential solutions for future sustainable energy systems.

3. Conclusion

Highly porous wood with nanofibril network filling in the lumen was synthesized by cell wall partial dissolution and regeneration using a one-step NaOH treatment for water evaporation-induced electricity harvesting. The high surface area and porosity act on the aqueous capillary flow and improve the solid/liquid interaction. Enhanced surface charge after NaOH treatment due to the generation of phenolic groups further contributes to power generation. Therefore, improved open-circuit potential and short-circuit current (≈10-fold) were observed for NaOH treated wood compared with native wood in water under neutral pH. When operating in alkali electrolyte reservoirs, an enhanced power generation was achieved with potential, current, and power density of ≈550 mV, ≈7 μA, and ≈620 nW cm^{-2}, respectively. Cycling test > 10 times show neither deterioration of the structure nor loss in performance. By further increasing the pH difference between wood (pH 1)

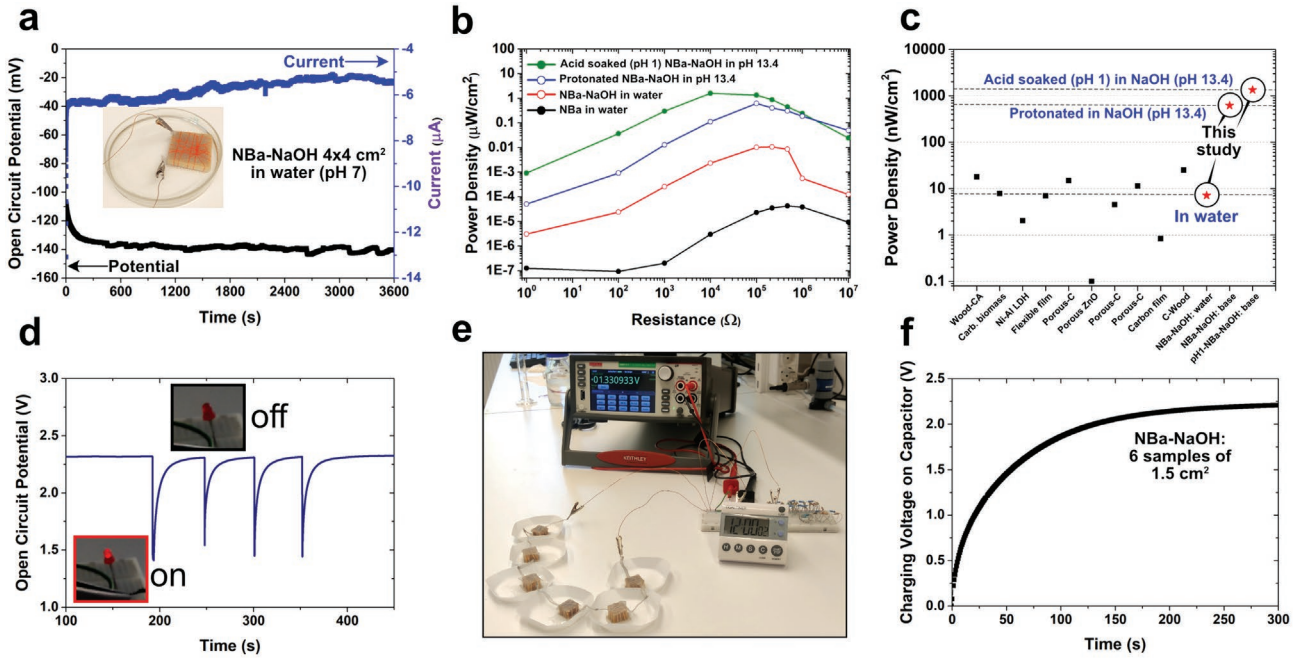

Figure 6. a) V_{oc} and I_{sc} of device based on 4 × 4 cm² NBa-NaOH in water. b) power density of devices based on 1.5 cm² NBa in water and device based on 1.5 cm² NBa-NaOH in water, pre-protonated run in pH 13.4 reservoir, and acid soaked run in pH 13.4 reservoir. c) Power densities of NBa-NaOH samples (1.5 cm²) in DI water, protonated and acid soaked before run in pH 13.4 reservoir and comparison with the literature reports.[5,10a–c,e,11,12c,25] d) LED lighting when circuit is connected and disconnected with six samples of 1.5 cm² based on protonated NBa-NaOH in pH 13.4 reservoir. e) powering a timer with six devices based on NBa-NaOH with 1.5 cm² area connected in series. f) charging of a capacitor using six NBa-NaOH samples with 1.5 cm² area.

and the water reservoir (pH 13.4) a V_{oc} of 1 V and a remarkable power output of 1.35 μW cm^{-2} was reached. Under the electrolyte conditions, the main source of electricity was appointed to the ion concentration gradient over the wood, where both surface chemistry and pH difference were critical for performance. The power generation could be easily scaled up by either using larger samples or connect small devices in series. The result in this work paves the way for sustainable energy systems development by using biomaterials through a scalable and green nanoengineering technology.

4. Experimental Section

Materials: Balsa wood (*Ochroma pyramidale*) of density 113 ± 3 kg m^{-3} was bought from Material AB, Sweden. Birch wood (*Betula pendula*, 658 ± 16 kg m^{-3}) was bought from Calexico wood AB, Sweden. Samples of dimensions 20 × 20 × 10 mm^3 (tangential × radial × axial) and 50 × 50 × 1 mm^3 cut for NaOH/water treatment. NaOH was bought from Sigma–Aldrich, Sweden and ethanol from VWR, Sweden.

Delignification of Balsa Wood: Balsa wood was delignified in 1 wt.% sodium chlorite in an acetate buffer (pH 4.6) solution at 80 °C for 18 h. Samples were re-introduced to a fresh solution every 6 h. Thereafter, the samples were washed repeatedly in deionized water.

Hydrogel and NaOH/Water Preparation: Pre-cooled water soaked wood (2–3 g at 2 °C) was introduced to a pre-cooled (−6 °C) NaOH/water solution containing 8 wt.% NaOH. Wood soaked in NaOH/water was kept at −6 °C for 48 h without agitation in which cellulosic and lignified components of the cell wall partially dissolved. Subsequently, the samples were kept at room temperature for 3 h to gel. During this time, a micro-phase separation of cellulose and NaOH happens and gradually transforms the wood from a semi-transparent partially dissolved state to a solid-like state,[26] which is usually called hydrogel. Thereafter, the samples were regenerated (a process wherein solubilized substance precipitate) in deionized water until neutral pH. During regeneration, dissolved cellulosic compound and lignin form nanofibrillated networks within the wood. Resultant samples had the suffix -NaOH.

Hydroelectricity – Setup and Generation: The device was prepared by sandwiching wood samples between two inert Pt meshes (nominal aperture 0.4 mm, wire diameter 0.1 mm, 20 × 20 mm^2) as current collector, as the wood was placed so that the microchannel direction was vertical relative the water reservoir, placed in a glass Petri dish. The Pt meshes were held tight to the wood using a thin cotton thread. The water reservoir level was ≈1–2 mm from the bottom of the glass dish using 20 mL DI water. All measured samples had an area of 1.5 cm^2 (radial: 1.5 cm^2 × tangential 1 cm^2) and thickness of 0.9 cm to assure standardized measurements. Prior to the device fabrication, the samples were washed using DI water (conductivity of 0.5–1 μScm^{-1}). When run in alkali electrolyte reservoir, the samples were first protonated in 0.1 M HCl (pH 1) for ≈3 h, thereafter, washed in DI water (until conductivity of 0.5–1 μScm^{-1}) and finally run in the alkali electrolyte of 0.26 M NaOH (pH 13.4). All alkali electrolyte measured samples were pre-protonated unless stated otherwise (e.g., as-prepared). When measuring acidified wood samples of pH 1 in alkali electrolyte (pH 13.4), the samples were treated in 0.1 M HCl (pH 1) for ≈3 h, followed by direct transfer into the alkali electrolyte reservoir. Large specimens had an area of 4 × 4 cm^2 and 0.9 cm thickness. The potential and current were recorded using an electrochemical work station (CHI Instruments, model 660E) and Keithley's DMM 7510 multimeter was used to measure the voltage, when simultaneous measurements were required. All the measurements were carried out at a constant temperature of 22 °C and 40% relative humidity.

Characterization: The sample morphology was observed in a field emission scanning electron microscopy (FE-SEM) using a Hitachi

S-4800, Japan. Wood cross-section was prepared by first treating the samples in a mixture of Water/Tert-butanol (50:50 vol%), thereafter freeze-fracturing them in liquid nitrogen (–196 °C) using a scalpel blade, followed by freeze-drying to dry them. All SEM analyzed samples were sputtered prior to analysis with a platinum/palladium layer of ≈3 nm, using a Cressington 208HR, UK, for 20 s.

The porosity of the specimen was calculated by using Equation 1, where the solid density of the specimen was measured with a pycnometer (Micromeritics Accupyc 1330, USA) and the bulk densities were calculated by drying the samples at 105 °C over-night followed by measuring the dimensions with a caliper and weighing the dry specimens.

$$\text{Porosity} = 1 - \frac{\text{Bulk density}\,\frac{\text{kg}}{\text{m}^3}}{\text{Solid density}\,\frac{\text{kg}}{\text{m}^3}} \quad (1)$$

Lignin and carbohydrate content was obtained by grinding the samples (Wiley mill), followed by hydrolyzing the material in sulphuric acid (73%). The hydrolyzed substance was thereafter filtered to separate the lignin from carbohydrates. Lignin content was subsequently obtained through the standard method: TAPPI T 222 om-2. The resultant filtered solution was introduced to a Dionex ICS-300 ion chromatography system (Thermo Fisher Scientific Inc.) to analyze the carbohydrate constituents.

Nanostructural characterization was performed by small angle X-ray scattering using a SAXSpoint, Anton Paar. Samples were run in DI-water, using a kapton film to seal the samples during measurements. The X-ray source was a supernova Copper of wavelength 1.541 Å, equipped with a Eiger R 1 M Horizontal detector. The 2D scattering reflection images were converted to 1D data using the software SAXSanalysis, wherein the water and Kapton film background was subtracted.

To preserve the nanostructure, specimen used for nitrogen physisorption measurements were dried using CO_2 supercritical point drying (Autosamdri-815, Tousimis, USA). Prior to drying, the samples were solvent exchanged to absolute ethanol. To obtain the specific surface area and pore-size distribution, nitrogen physisorption was performed at 77 k using a Micromeritics ASAP 2020. Samples were analyzed between the relative pressures 0.05–1.0 P/P_0 in liquid nitrogen (–196 °C). SSA was determined between the relative pressures 0.05–0.25, using the BET theory[27] and pore-size distribution was determined from the desorption isotherm using the Barret–Joyner–Halenda model.

Chemical functionalities were characterized using an attenuated total reflectance Fourier transform infrared (ATR-FTIR), performed on a PerkinElmer Spectrum 100 FTIR spectrometer equipped with an MKII Golden Gate, single-reflection accessory unit with a diamond ATR crystal (Graseby Specac LTD, England). The spectra were attained over the range of 4000–600 cm^{-1} using eight consecutive scans.

Total charge of the wood samples was measured using conductometric titration on a Metrohm 702SM Titrino titrator (Switzerland), according to the standard SCAN-CM 65:02, repeated 3 times for each specimen.

The ζ-potential was measured three times for each sample, using a Zetasizer Nano ZSE (Malvern Instrument Ltd., U.K.). Prior to analysis a 0.1 wt.% suspension was prepared for each sample using a kitchen blender, wherein the supernatant phase was measured. ζ-potential titrations were conducted on a Zetasizer Advance Series Pro Red integrated to an MPT-3 Multi-purpose Titrator accessory (Malvern Instruments Ltd., U.K.).

Milled wood lignin (MWL) extraction was performed by mechanical pretreatment of wood according to previous work with some modifications.[28] In short, birch wood was milled in a Wiley Mini-Mill 3383-L70 (Thomas Scientific, USA), through a 20-mesh. The wood ground was further milled in a Retsch PM400 (Ninolab, Sweden) for 24 h using 1 h milling intervals with 30 min pauses. The grinding jar was purged with nitrogen prior to milling. In the case of the NBa-NaOH sample, 1 g was ball milled in an 80 mL stainless steel jar, using 10 stainless steel grinding balls. For the extraction of MWL both from birch and the NBa-NaOH, the Björkman protocol was used with some modifications.[29] Ball milled birch (3 g) were mixed with 96% (v/v) 1,4-dioxane (Sigma–Aldrich, Sweden) (75 mL) for 72 h, at room temperature. In the case of NBa-NaOH, 800 mg of the ball milled material was extracted with 45 mL 96% (v/v) 1,4-dioxane. In both experiments, the extract was collected by centrifugation and the dioxane was completely removed under reduced pressure in a rotary evaporator. MWL was further treated with NaOH for 48 h at –6 °C to mimic the cold water/NaOH process. In order to collect lignin, the pH of the lignin solution was adjusted to pH 2 with the addition of HCl. The precipitated lignin was collected by centrifugation and washed twice with Milli-Q water (pH 4). The product was then freeze-dried. Acetylation of lignin is needed for the SEC measurements. Acetylation of lignin was performed following the protocol by Gellerstedt with some modifications as reported in previous work.[28,30] In short, 2 mg of the material was mixed with 100 µL of pyridine and acetic anhydride (Sigma–Aldrich, Sweden) in 1:1 ratio, overnight, at room temperature. The solution was dried under nitrogen flow. Pyridine was efficiently removed by addition of a cold methanol and toluene solution (Sigma–Aldrich, Sweden), in 1:1 ratio.

A gel permeation chromatography (GPC) system from Waters (Waters Sverige AB, Sollentuna, Sweden) was used for the characterization of the molecular weight of the lignin. The system consists of a Waters- 515 high pressure liquid chromatography (HPLC) pump, a 2707 autosampler, a 2998 photodiode array detector (254 and 280 nm) and a 2414 refractive index (RI) detector. Waters Ultrastyragel HR4, HR2, and HR0.5 (4.6 × 300 mm) solvent efficient columns were used, connected in series. A Styragel guard column was used. The columns were thermostated at 35 °C. Polystyrene standards with molecular weights from 176 kDa to 370 Da were used for the calibration. The solvent (tetrahydrofuran) flow rate was 0.3 mL min^{-1}.

^{31}P-NMR experiments were performed according to previous work,[31] following the protocol developed by Argyropoulos.[32] In short, 30 mg of the product were mixed with 200 µL dimethylformamide and pyridine in 1:1 ratio until complete dissolution. 50 µL of an internal standard solution comprised of endo-N-Hydroxy-5-norbornene-2,3-dicarboximide in pyridine (60 mg mL^{-1} pyridine) and a relaxation agent, $Cr(AcAc)_3$ (5 mg mL^{-1} pyridine). A mixture of the phosphorylation agent 2-chloro-4,4,5,5-tetramethyl-1,3,2-dioxaphospholane (100 µL) and d_3-$CDCl_3$ (450 µL) was added to the sample solution and the reaction proceeded for 1 h before NMR analysis. The NMR analysis was performed on a Bruker Avance III HD 400 MHz instrument with a BBFO probe equipped with a Z-gradient coil. For the experiment, the pulse sequence zgig30 was used, with 256 number of scans, and a relaxation delay (D1) of 5 s. The spectra were processed with MestreNova (Mestrelab Research).

Supporting Information

Supporting Information is available from the Wiley Online Library or from the author.

Acknowledgements

Vetenskapsrådet (VR, No. 2017-05349) and Knut & Alice foundation through the Wallenberg Wood Science Center and European Research Council (ERC) under the European Union's Horizon 2020 research and innovation programme (No. 742733) are acknowledged. The authors are also grateful for the support of Treesearch through the Research Infrastructure access program. Special thanks to professor Lars A. Berglund for his kind support and to Professor Lars Wågberg for the scientific discussions. Associate professor Jiantong Li is acknowledged for the help of Pt mesh current collector preparation.

Conflict of Interest

The authors declare no conflict of interest.

Data Availability Statement

The data that support the findings of this study are available from the corresponding author upon reasonable request.

Keywords

cell wall nanoengineering, green chemistry, water evaporation, wood power generators

Received: August 3, 2022
Revised: November 2, 2022
Published online:

[1] Z. Zhang, X. Li, J. Yin, Y. Xu, W. Fei, M. Xue, Q. Wang, J. Zhou, W. Guo, *Nat. Nanotechnol.* **2018**, *13*, 1109.
[2] J. Yin, J. Zhou, S. Fang, W. Guo, *Joule* **2020**, *4*, 1852.
[3] a) R. Kumar, T. Tabrizizadeh, S. Chaurasia, G. Liu, K. Stamplecoskie, *Sustainable Energy Fuels* **2022**, *6*, 1141; b) L. Li, S. Feng, Y. Bai, X. Yang, M. Liu, M. Hao, S. Wang, Y. Wu, F. Sun, Z. Liu, T. Zhang, *Nat. Commun.* **2022**, *13*, 1043.
[4] J. Yin, Z. Zhang, X. Li, J. Yu, J. Zhou, Y. Chen, W. Guo, *Nat. Commun.* **2014**, *5*, 3582.
[5] G. Xue, Y. Xu, T. Ding, J. Li, J. Yin, W. Fei, Y. Cao, J. Yu, L. Yuan, L. Gong, J. Chen, S. Deng, J. Zhou, W. Guo, *Nat. Nanotechnol.* **2017**, *12*, 317.
[6] a) Y. Li, J. Cui, H. Shen, C. Liu, P. Wu, Z. Qian, Y. Duan, D. Liu, *Nano Energy* **2022**, *96*, 107065; b) F. Zhao, H. Cheng, Z. Zhang, L. Jiang, L. Qu, *Adv. Mater.* **2015**, *27*, 4351.
[7] a) J. H. Lee, S. Kim, T. Y. Kim, U. Khan, S.-W. Kim, *Nano Energy* **2019**, *58*, 579; b) J. Yin, X. Li, J. Yu, Z. Zhang, J. Zhou, W. Guo, *Nat. Nanotechnol.* **2014**, *9*, 378.
[8] a) K. Xiao, L. Jiang, M. Antonietti, *Joule* **2019**, *3*, 2364; b) J. Yang, F. Z. Lu, L. W. Kostiuk, D. Y. Kwok, *J. Micromech. Microeng.* **2003**, *13*, 963.
[9] W. Olthuis, B. Schippers, J. Eijkel, A. van den Berg, *Sens. Actuators, B* **2005**, *111*, 385.
[10] a) T. P. Ding, K. Liu, J. Li, G. B. Xue, Q. Chen, L. Huang, B. Hu, J. Zhou, *Adv. Funct. Mater.* **2017**, *27*, 1700551; b) T. Y. Zhong, H. Y. Guan, Y. T. Dai, H. X. He, L. L. Xing, Y. Zhang, X. Y. Xue, *Nano Energy* **2019**, *60*, 52; c) J. Li, K. Liu, T. Ding, P. Yang, J. Duan, J. Zhou, *Nano Energy* **2019**, *58*, 797; d) C. Li, Z. Tian, L. Liang, S. Yin, P. K. Shen, *ACS Appl. Mater. Interfaces* **2019**, *11*, 4922; e) H. He, T. Zhao, H. Guan, T. Zhong, H. Zeng, L. Xing, Y. Zhang, X. Xue, *Sci. Bull.* **2019**, *64*, 1409; f) B. Hou, Z. Cui, X. Zhu, X. Liu, G. Wang, J. Wang, T. Mei, J. Li, X. Wang, *Mater. Chem. Phys.* **2019**, *222*, 159.
[11] a) C. Shao, B. Ji, T. Xu, J. Gao, X. Gao, Y. Xiao, Y. Zhao, N. Chen, L. Jiang, L. Qu, *ACS Appl. Mater. Interfaces* **2019**, *11*, 30927; b) S. G. Yoon, Y. Yang, J. Yoo, H. Jin, W. H. Lee, J. Park, Y. S. Kim, *ACS Appl. Electron. Mater.* **2019**, *1*, 1746; c) J. C. Sun, P. D. Li, J. Y. Qu, X. Lu, Y. Q. Xie, F. Gao, Y. Li, M. F. Gang, Q. J. Feng, H. W. Liang, X. C. Xia, C. R. Li, S. C. Xu, J. M. Bian, *Nano Energy* **2019**, *57*, 269; d) B. Ji, N. Chen, C. Shao, Q. Liu, J. Gao, T. Xu, H. Cheng, L. Qu, *J. Mater. Chem. A* **2019**, *7*, 6766.
[12] a) X. Liu, H. Gao, J. E. Ward, X. Liu, B. Yin, T. Fu, J. Chen, D. R. Lovley, J. Yao, *Nature* **2020**, *578*, 550; b) X. Zhou, W. Zhang, C. Zhang, Y. Tan, J. Guo, Z. Sun, X. Deng, *ACS Appl. Mater. Interfaces* **2020**, *12*, 11232; c) Z. M. Zhang, Y. R. Zheng, N. Jiang, W. Q. Hong, T. Y. Liu, H. Jiang, Y. J. Hu, C. Z. Li, *Sustainable Energy Fuels* **2022**, *6*, 2249; d) Q. Hu, Y. Ma, G. Ren, B. Zhang, S. Zhou, *Sci. Adv.* **2022**, *8*, eabm8047.
[13] J. N. Israelachvili, in *Intermolecular and Surface Forces*, 3rd ed. (Ed: J. N. Israelachvili), Academic Press, San Diego **2011**, p. 291.
[14] a) J. Garemark, J. E. Perea-Buceta, D. Rico Del Cerro, S. Hall, B. Berke, I. Kilpelainen, L. A. Berglund, Y. Li, *ACS Appl. Mater. Interfaces* **2022**, *14*, 24697; b) J. Garemark, X. Yang, X. Sheng, O. Cheung, L. Sun, L. A. Berglund, Y. Li, *ACS Nano* **2020**, *14*, 7111.
[15] T. Budtova, P. Navard, *Cellulose* **2016**, *23*, 5.
[16] A. A. Modenbach, S. E. Nokes, *Trans. ASABE* **2014**, *57*, 1187.
[17] a) H. F. Jakob, S. E. Tschegg, P. Fratzl, *Macromolecules* **1996**, *29*, 8435; b) P. Chen, Y. Li, Y. Nishiyama, S. V. Pingali, H. M. O'Neill, Q. Zhang, L. A. Berglund, *Nano Lett.* **2021**, *21*, 2883; c) P. Penttilä, L. Rautkari, M. Österberg, R. Schweins, *J. Appl. Crystallogr.* **2019**, *52*, 369.
[18] a) H. F. Jakob, D. Fengel, S. E. Tschegg, P. Fratzl, *Macromolecules* **1995**, *28*, 8782; b) J. C. Hiller, T. J. Thompson, M. P. Evison, A. T. Chamberlain, T. J. Wess, *Biomaterials* **2003**, *24*, 5091.
[19] V. Lutz-Bueno, A. Diaz, T. Wu, G. Nystrom, T. Geiger, C. Antonini, *Biomacromolecules* **2022**, *23*, 676.
[20] C. J. Knill, J. F. Kennedy, *Carbohydr. Polym.* **2003**, *51*, 281.
[21] L. Tan, Y.-Q. Tang, H. Nishimura, S. Takei, S. Morimura, K. Kida, *Prep. Biochem. Biotechnol.* **2013**, *43*, 682.
[22] C. H. Hamann, in *Electrochemistry* (Eds: A. Hamnett, W. Vielstich), Wiley-VCH, Weinheim **1998**, pp. 13–65.
[23] a) W. Sparreboom, A. van den Berg, J. C. T. Eijkel, *Nat. Nanotechnol.* **2009**, *4*, 713; b) C. L. Rice, R. Whitehead, *J. Phys. Chem.* **2002**, *69*, 4017.
[24] a) H. H. Cheng, Y. X. Huang, F. Zhao, C. Yang, P. P. Zhang, L. Jiang, G. Q. Shi, L. T. Qu, *Energy Environ. Sci.* **2018**, *11*, 2839; b) T. Xu, X. T. Ding, Y. X. Huang, C. X. Shao, L. Song, X. Gao, Z. P. Zhang, L. T. Qu, *Energy Environ. Sci.* **2019**, *12*, 972.
[25] a) G. Zhou, Z. Ren, L. Wang, J. Wu, B. Sun, A. Zhou, G. Zhang, S. Zheng, S. Duan, Q. Song, *Nano Energy* **2019**, *63*, 103793; b) H. Guan, T. Zhong, H. He, T. Zhao, L. Xing, Y. Zhang, X. Xue, *Nano Energy* **2019**, *59*, 754; c) K. Liu, T. Ding, J. Li, Q. Chen, G. Xue, P. Yang, M. Xu, Z. L. Wang, J. Zhou, *Adv. Energy Mater.* **2018**, *8*, 1702481; d) G. Zhang, Y. Xu, Z. Duan, W. Yu, C. Liu, W. Yao, *Appl. Therm. Eng.* **2020**, *166*, 114623.
[26] R. Gavillon, T. Budtova, *Biomacromolecules* **2008**, *9*, 269.
[27] S. Brunauer, P. H. Emmett, E. Teller, *J. Am. Chem. Soc.* **1938**, *60*, 309.
[28] I. Sapouna, M. Lawoko, *Green Chem.* **2021**, *23*, 3348.
[29] A. Björkman, *Nature* **1954**, *174*, 1057.
[30] C. Gioia, G. Lo Re, M. Lawoko, L. Berglund, *J. Am. Chem. Soc.* **2018**, *140*, 4054.
[31] D. Argyropoulos, *J. Wood Chem. Technol.* **1994**, *14*, 45.